International Journal of Nanoelectronics and Materials
IJNeaM
ISSN 1985-5761 | E-ISSN 2232-1535

Effects of UV Laser Radiation and Soft Lithographic Patterning on the Wettability of Silk Thin Films

A. F. Mohammed[a,*], Q. Aljarwani[b], A. Aesa[c], C. D. Walton[d]

[a]*Applied Science College, University of Technology- Iraq, Baghdad, Iraq*
[b]*Material Engineering College, University of Babylon, Babylon, Iraq*
[c]*Department of Physics, College of Science, University of Kirkuk, Kirkuk, Iraq*
[d]*School of Mathematics and Physical Sciences, Hull University, HU6 7RX, UK*
**Corresponding author. Tel.: +9647736791147; E-mail: 100009@uotechnology.edu.iq*

ABSTRACT

Liquid interaction with solids is crucial to optimize material design and processes across many applications. Therefore, wettability is of significant importance in such interactions. This study investigates the impact of an excimer laser of 193 nm wavelength patterned Silk fibroin (SF) films. Various techniques were employed to characterize the SF films, including AFM, SEM, and WLI. A UV–visible spectrophotometer was utilized to assess the morphological and optical characteristics of the SF films. Laser structuring generated periodic gratings (5–10 μm) and increased surface roughness, reducing water contact angles by 50%—indicating a dramatic wettability shift from hydrophobic to hydrophilic behavior. The films exhibited strong UV absorption ($\alpha = 7.3\times10^4$ cm^{-1}) while maintaining optical clarity in visible wavelengths, ideal for light-guiding applications. AFM and SEM revealed that laser patterning softened the SF matrix and introduced micro/nanoscale topography, directly correlating with a 40–50% increase in surface energy (WLI-validated). These modifications enable precise liquid-surface interactions critical for biosensor interfaces, drug-eluting coatings, or cell-adhesive substrates. The combined optical tunability (UV-Vis) and wettability control (contact angle: 90° → 45°) position laser-patterned SF films as a dual-functional platform for lab-on-chip devices or implantable photonic therapeutics.

Keywords: *Wettability, Contact angle, Surface energy, Silk Fibroin, Laser ablation, 193 nm laser*

1. INTRODUCTION

Laser modifications of biological materials, such as proteins, is being developed for various bio applications**.** Lasers were used to synthesise the protein silk fibroin (SF) [1–5]. Moreover, different laser wavelengths have been used to modify the SF and characterize the effect of pulsed laser on the material [6-9]. Silk, also known as fibroin fiber, is a natural protein produced by insects such as spiders' or worms' cocoons. Silk consists of two proteins: the heavy and light fibroin chains**,** along with sericin, which crosslinks the fibroin to form the cocoon [10-15].

Silk fibroin fibers are among the strongest biomaterials, known for their high toughness, biocompatibility, biodegradability, and excellent optical properties. Fibroin films are transparent across visible wavelengths until the mid-infrared region can be implanted or produced as free-standing films, and remain thermally stable in ambient conditions [16–18].

Due to these high-quality properties, silk fibroin can be used for many applications [19–24] , including biophotonic applications that combine biology and optics. It can be fabricated into various structures such as thin films, diffraction grating (high-resolution, fewer than 20 nm), photonic crystals, organic crystals (i.e. bioactive optical filters), waveguides, biosensors, bio-detectors, and microfluidic chambers [25-29]. It also has an application in medicine and drug delivery [30, 31].

Silk fibroin possesses a unique combination of hydrophobic and hydrophilic properties. The sericin proteins are hydrophilic, whilst hydrophobic sequences dominate the β-sheet-crystalline regions of fibroin [32, 33]. The beta-sheets within silk fibroin make it highly resistant to water, and even solvents, such as formic acid, will not completely dissolve it [34, 35]. Surface wettability has attracted a significant research attention, as it is possible to alter it by controlling the material surface and so allowing the material to be used in different applications [36, 37]. Furthermore, a material's wettability significantly influences its biophotonic properties. Wettability refers to a liquid's ability to spread across a solid surface, typically quantified by measuring the contact angle formed at the intersection of liquid/air and solid/liquid interfaces [38-40].

2. THEORETICAL BACKGROUND

On an ideal surface (homogeneous, smooth, flat), the contact between the surface and the liquid can have different shapes and angles of contact Figure 1. Contact angle represents the angle controlled by two interfaces, that of the liquid/solid and liquid/gas. If the contact angle is $\theta>90^o$, then it is a hydrophobic surface. A neutral surface

has a contact angle of θ=90°. A surface with θ<90° is called hydrophilic, and a perfect wetting surface has a θ=180° 41-43]. The contact angle at equilibrium is calculated by the Young equation (Eq 1) [44-47].

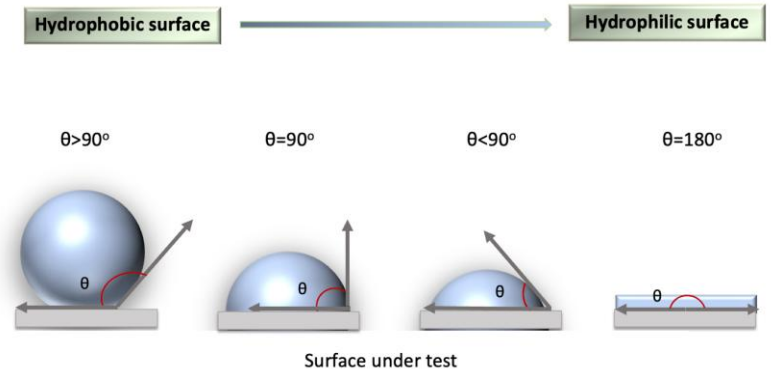

Figure 1. Young Model contact angle schematic behaviour of liquid on the surface. Non-wetting behaviour for θ>90°, Neutral for θ=90°, good wetting for θ<90° and perfect wetting for θ<<90°.

$$\gamma_{SG} = \gamma_{SL} - \gamma_{LG}\cos\theta \quad (1)$$

Where θ is the contact angle and γ_{SG}, γ_{SL} and γ_{LG} are the interfacial tensions of the liquid vapour phase, solid/vapour phase, and solid/liquid, respectively. For the non-ideal solid surface Figure 2, with higher roughness than the homogeneous, flat surface, the situation is more complicated because the surface area is increased, and sharp edges exist [48, 49]. Therefore, the contact angle has to be evaluated by the Wenzel model (Eq 2) [50, 51]. He assumed that a surface roughness would increase the liquid-solid surface area. This has more influence on the good wettability surfaces than the poor ones, where the droplets don't go all the way to the surface and instead form air pockets [52, 53]. Wenzel, in 1936, articulated the relation between roughness and wettability. He explained that increasing the surface texture would change the wettability behaviour caused by the surface chemistry (i.e., the hydrophobic surface would increase in hydrophobicity) [54-56].

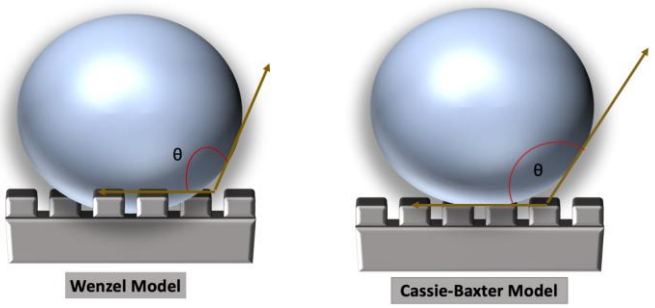

Figure 2. Schematics of wettability models: Wenzel's homogeneous wetting regime (left) and Cassie-Baxter's heterogeneous composite state (right), illustrating how surface roughness influences liquid droplet behavior. Arrows denote contact angle transitions due to microstructural features.

$$\cos\theta_w = R\cos\theta \quad (2)$$

is called the roughness factor (the ratio between the actual surface area and the apparent surface, $R \geq 1$), and θ_w *is the apparent contact angle*. If R=1, that means the apparent contact angle and the actual angle are the same as the surface is smooth. This equation is used for droplets with no trapped air. It is crucial to acknowledge that the Wenzel equation is predicated upon the assumption that the liquid entirely infiltrates the grooves of roughness. The Wenzel equation serves as an approximation that becomes increasingly precise as the droplet dimensions exceed the scale of the surface roughness. Consequently, if the droplet size surpasses the roughness scale by two to three orders of magnitude, the application of the Wenzel equation is warranted. Furthermore, owing to its elevated band gap, the electronic and optical characteristics are significantly enhanced.

However, when air pockets exist in the roughness texture under the liquid, the wettability Wenzel equation will be derived into the Cassie-Baxter equations [57-59]:

$$\cos\theta_A = R.\Phi_{SL}[\cos\theta + 1] - 1 \quad (3)$$

Where θ_A represents the apparent contact angle, Φ_{SL} is the solid surface fraction ($0 \le \Phi_{SL} \le 1$). Surfaces with superhydrophobicity form air pockets beneath their droplet.

The surface tension could be determined by the contact angle and, thus, the wettability. The surface energy well defines the surface tension of a droplet. Surface tension is defined as the intermolecular forces that control the droplet shape [43, 60].

In this work, both the contact angle and the surface energy of droplets on SF films were studied. Furthermore, a 193 nm excimer laser was employed to alter the surface texture of the SF films to study the effect of roughness on its wettability characterisation. The silk fibroin films were studied before and after irradiation. Silk has been reported to have good wettability with a contact angle of about 60°-70° [61, 62]. Other studies show a change in hydrophobicity when changing a silk fibroin film surface [63, 64].

3. METHODOLOGY

BioMatrix's silk solution, containing approximately 50 mg/mL (5% W/V) of solubilized protein with an approximate molecular weight of 100 kDa, was utilized. This silk solution is exclusively composed of 100% fibroin protein sourced from the domesticated Bombyx mori silkworm. Careful handling of this solution is needed, as it necessitates storage at temperatures between -60°C and -70°C [65]. This solution must be allowed to attain room temperature gradually over several hours. The fabrication of silk films is achieved by depositing the fibroin solution onto a fused silica substrate utilizing a spin-coating technique at a 250 rpm rotational speed for 30 seconds. Subsequently, the solution was air-dried, allowing the crystallization process to form a film. The resultant thicknesses of the films were engineered to range from a few nanometers to several micrometers. These films exhibit a uniform and smooth morphology, characterised by a surface roughness measuring 3-4 nm due to the controlled drying process.

Characterization of the films was conducted utilizing UV-Vis spectroscopy (Thermo Scientific, Evolution 220) to investigate the synthesized SF film transmittance and absorbance. The absorption coefficient was derived from the optical spectra using the equation $\alpha=2.303A/t$, where A represents absorbance, and t denotes the film thickness [44]. The roughness and texture of these films were analyzed by Atomic Force Microscopy (AFM)(Bruker edge).

For the determination of contact angle and surface energy, a sessile drop device (goniometer OCA100; DataPhysics Instruments GmbH, Germany) integrated with SCA20 software was utilized. Triple distilled water (TDI) served as the probe liquid, with a volume of 5 µl administered onto the fibroin surface. Subsequently, an additional 2-5 µl of TDI water was added. Liquid addition resulted in the advance of the triple line, allowing for the measurement of the advanced dynamic contact angle. Five dynamic contact angles were recorded and utilized to compute the average contact angle for the surface. The evaluation of surface free energy was conducted using the SCA20 software following the Equation of State method.

The optical grating was subsequently executed via laser irradiation employing an excimer laser (Lambda Physik LPF 202) of 193 nm wavelength with a 11.5 nm pulse duration. The laser light was reimaged (5-factor demagnification) with a parallel bar grid customised by (Agar Co, 400 Parallel Bar Nickel 3.05 mm diameter: AGG2016N), with a static ablation site of 390 µm. The applied laser fluence was 28 $mJcm^{-2}$, with an Aerotech nano stage (Aerotech Fibre Align) operating at a 0.1 mms^{-1} velocity. [66-68] The control of laser fluence was managed by an attenuator (Metrolux, ML2110) and measured utilising a Joulemeter (Molectron). The characterisation of the created grating was performed using Scanning Electron Microscopy (SEM) (SEM, Zeiss EVO60) and a White Light Interferometer (WLI, WYKO NT1100).

4. DISCUSSION AND RESULTS

Several characterisations were conducted to investigate the silk surface before the laser texturing. The transmittance and absorbance of the silk fibroin were conducted using a UV-visible spectrometer Figure 3. The SF was found to be transparent (~99%) in the visible spectrum and near-infrared spectra (300–1100 nm), with a dramatic drop in transparency in the UV range (<300 nm), which was the result of protein absorbance.

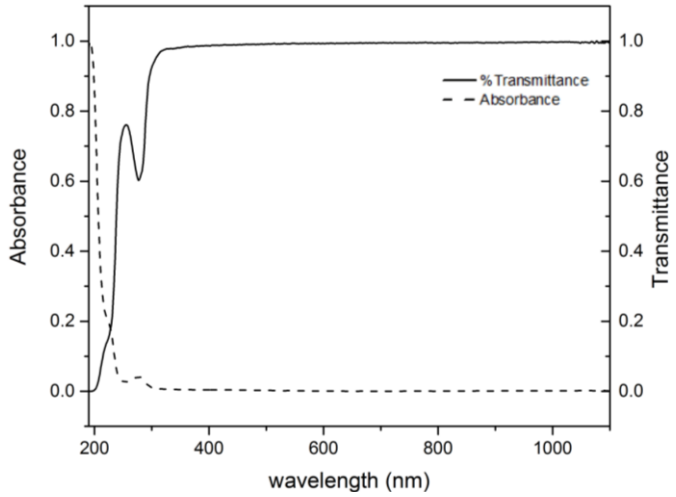

Figure 3. UV-Vis spectra across 200-1000 nm wavelengths. The plot demonstrates high absorbance in the UV region (200-400 nm) and increased transparency in the visible to NIR range (600-1000 nm).

The transmittance of silk fibroin exhibits a direct correlation with the methodology used in its fabrication. In the present study, the observed transmittance was higher than the values documented in previous research [62]. This elevated transmittance within the visible spectrum provides a solid ground for its application in optical devices, such as gratings. Furthermore, from the above measurements, SF's absorption coefficient at (193 nm) was derived to be approximately $\alpha \sim 7.3 \times 10^4$ cm^{-1}, as illustrated in Figure 4.

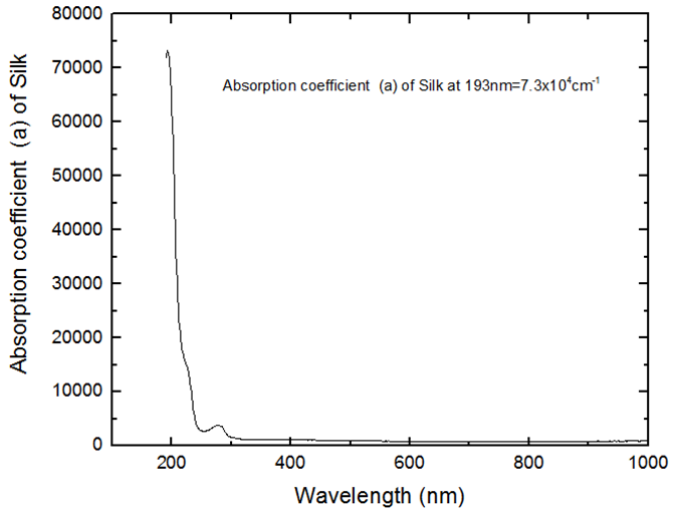

Figure 4. Absorption coefficient (α) spectrum of silk, showing strong UV absorption with $\alpha = 7.3 \times 10^4$ cm^{-1} at 193 nm.

AFM was employed to analyze the topography of the surface after preparation. The AFM was operated in tapping mode utilizing "unmounted high-quality Pyramidal Silicon Tips" (Tespa-V2 with 8 nm radius) to characterize the roughness of the surface within a designated area of 10×10 µm. The roughness is significantly influenced by the grating pitch and depth, controlling the extent of the surface area subjected to interacting liquids. Another crucial aspect of the grating is the periodic patterns that regulate the interval between the grating lines and directly affect how fluids and light interact with the material's surface. A reduced pitch may lead to enhanced capillary phenomena concerning wettability, which can alter the behaviour of fluids in terms of their dispersion or the formation of droplets on the surface. This consideration is particularly relevant for systems such as microfluidics, where precise fluid management is essential [59].

The AFM micrographs exhibit the occurrence of small-scale elevations and columns, with roughness measurements varying between 3-4.5 nm, refer to Figure 5. Furthermore, Figure 6 illustrates the depth of the prepared grating as quantified by White Light Interferometry (WLI). The channel widths were determined via the employed objective mask, ranging between 5-10 µm. The channels were determined to possess a depth of 0.25 µm, corresponding to the mentioned laser operational parameters. These findings were substantiated by scanning electron microscopy images in Figure 7.

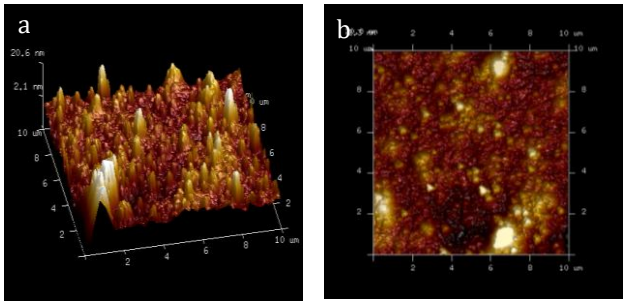

Figure 5. AFM micrographs of the SF surface a) 3D image for an area of 10×10 μm b) top view of the film for the same area.

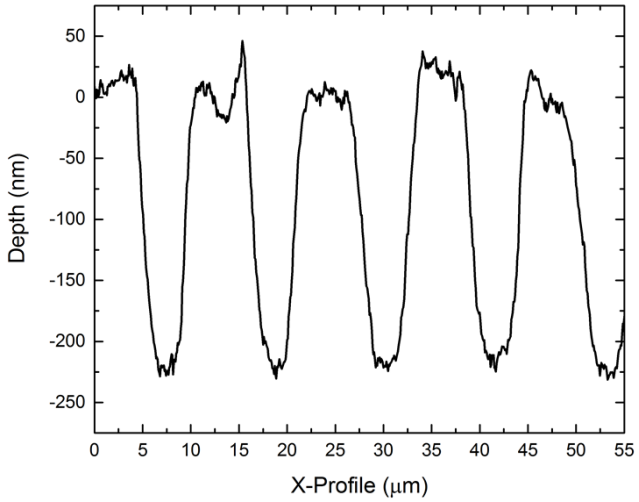

Figure 6. Cross-sectional 1D stylus profile measurement of the created grating by 193 nm laser of SF. The channel depth was 250 nm and a width of 5-10 μm. The X-profile reveals nanoscale surface roughness characteristic of spin-coated or solvent-cast fibroin layers.

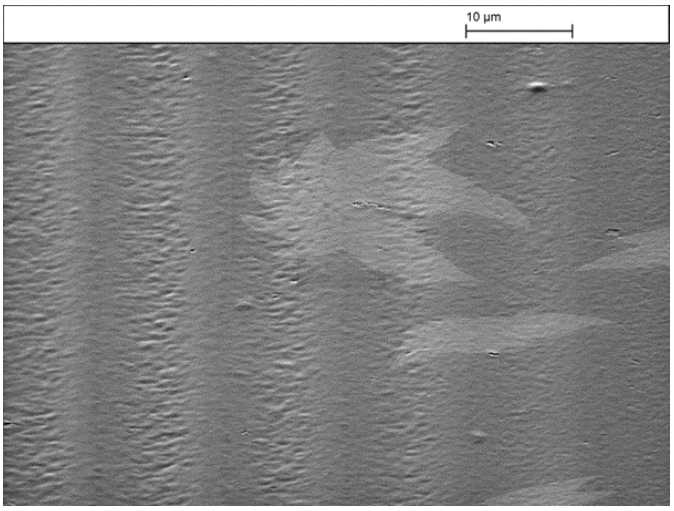

Figure 7. SEM micrograph of the grating produced by 193 nm laser ablation of SF. The ablated SF thickness was 475 nm. The film was created with a laser fluence of 28 mJcm^{-2}.

Despite the robustness of the film, the rapid thermal excitation from the laser facilitated the ablation of the film. The silk fibroin film has been documented as a resilient and stable protein that does not undergo melting due to thermal exposure. However, it has been demonstrated to melt under specific conditions, as explained by [15]. The lighter regions observed in Figure 7 may be attributed to the fact that silk fibroin exhibits various crystallization phases or the heterogeneity of the film.

Figure 8 demonstrates the measured contact angle for silk fibroin, both in its prepared state and after grating via a 193 nm laser, as determined through the sessile drop technique. The measurement was conducted repetitively. The obtained data indicates that the contact angles of silk fibroin prior to irradiation ranged from 41° to 61°, with an average contact angle of 47.8°. The contact angles recorded post-laser irradiation, following the formation of the grating, were found to range between 19.7° and 31.2°, with

an average contact angle of 25.8°. This observation signifies that the grating structure resulted in a 50% reduction in the contact angle.

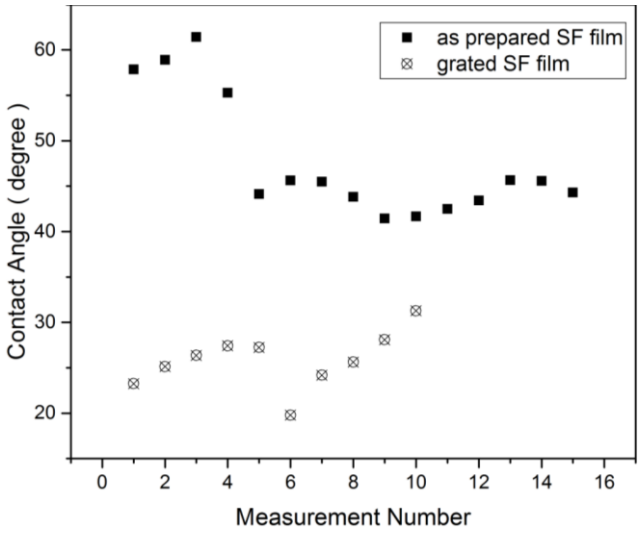

Figure 8. Average water contact angle of silk fibroin films before (47.8° ± X°) and after (25.8° ± X°) 193 nm laser irradiation, measured using the sessile drop technique (n=5).

It is believed that these outcomes are indicative of the Cassie-Baxter model. The same concepts were applied to the surface energy measurements Figure 9.

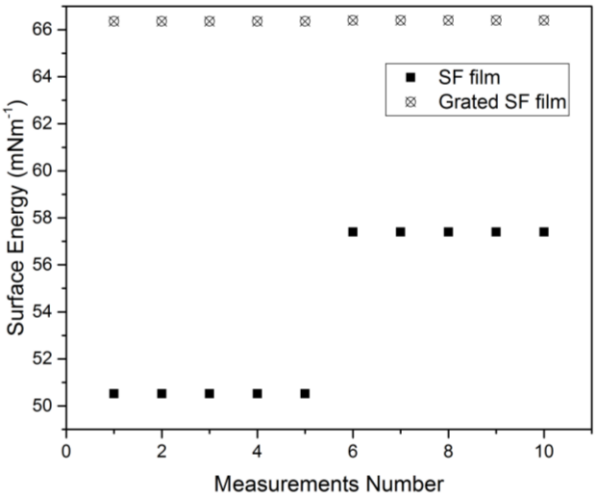

Figure 9. Surface energy measurements of pristine silk fibroin (SF) films (52–56 mN/m) versus grated SF films (58–60 mN/m), showing increased surface energy after physical modification. Data points represent 10 consecutive measurements per sample type.

The free surface energy measurements were conducted twice for the prepared silk fibroin film, valued at 50.5 mNm^{-1} and 57.4 mNm^{-1}. A singular measurement of the surface energy was recorded following the grating process via the 193 nm laser. It was calculated to be 66.4 mNm^{-1}, representing an increase relative to the surface free energy of the non-grated SF. Therefore, it was found that the transition of the surface from a nanometer-scale roughness to a micrometer-scale structure induced by grating resulted in a decreased contact angle and enhanced the hydrophobic character of the surface. Additionally, this modification correlated with an increase in free surface energy. Upon the grated microchannel, the irregularity of the surface increased, thus reducing wettability. This can be attributed to the elevation of the contact angle at a more textured surface. Wenzel and Cassie–Baxter models exhibit the influence of roughness on wettability phenomena. Following the grating process, the SF surface could have transitioned into a state wherein air pockets are trapped by surface grooves and irregularities, aligning closely with the Cassie–Baxter model. In surfaces subjected to excimer laser treatment, there is an observed increase in surface-free energy due to enlarged surface area, coupled with a potential rise in the number of reactive sites. On softer substrates, a higher surface-free energy typically correlates with improved wettability. Elevated surface energy on a

roughened surface may result in more pronounced air interaction and, consequently, an increased contact angle [69, 70].

5. CONCLUSION

It has been established that each surface exhibits a distinct degree of hydrophobicity. By altering the surface roughness from the nanometre scale to the micrometre scale through the application of laser grating techniques, a decrease in hydrophobicity can be observed, indicated by a reduction in the contact angle. In comparison, an enhancement in surface energy was noted.

The roughness of the spin-coated SF film was determined to average 4 nm as assessed by (AFM). This measurement was recognised as the smoothest surface achieved via the spin coating methodology. Within this roughness range, wettability was minimal, and it decreased further when 5-10 μm channels were produced on the surface.

Researchers and technicians possess the capability to control the surface free energy by modifying surface roughness to optimise wettability based on defined criteria. It has been observed here that the wettability of Silk Fibroin films, even at minimal surface roughness values, is subject to alterations due to fluctuations in roughness. The architecture of the SF grated films was determined to reduce the liquid θ, thereby signifying an improvement in wettability. Furthermore, it is essential to comprehend how the grating dimensions, including (width, height, shape), and grating periodicity, influence the Wenzel and Cassie–Baxter states of the water contact. Grating dimensions may employed to customise the wettability of solid interfaces.

Patterned films elevate the surface free energy, thereby emphasising the complex interrelationship between wettability and surface roughness. Consequently, this study offers significant insights into the modification of surface properties of SF films through laser texturing, which possesses prospective applications across a diverse range of fields, such as protective coatings and medical devices.

ACKNOWLEDGMENTS

Acknowledgments may be inserted at the end of the paper, before the references, not as a footnote to the title. Use the unnumbered Acknowledgements Head style for the Acknowledgments heading

REFERENCES

[1] Y. Tsuboi, H. Adachi, K. Yamada, H. Miyasaka, and A. Itaya, "Laser ablation of silk protein (fibroin) films," *Japanese J. Appl. Physics, Part 1 Regul. Pap. Short Notes Rev. Pap.*, vol. 41, no. 7 A, pp. 4772–4779, 2002, doi: 10.1143/JJAP.41.4772.

[2] Fakhri M. A.; Al-Douri Y.; Hashim U., Fabricated Optical Strip Waveguide of Nanophotonics lthium Niobate, IEEE Photonics Journal, 8(2), 7409919 (2016) 10.1109/JPHOT.2016.2531583.

[3] M. G. and A. I. Y. Tsuboi, "Thin Film Formation of a Protein by Laser Ablation Deposition Technique," *Chemistry letters*. 1998.

[4] Zainab T. Hussain, Khawla S. Khashan, Rana O. Mahdi, Characterization of cadmium oxide nanoparticles prepared through Nd:YAG laser ablation process, Materials Today: ProceedingsVolume 42, Pages 2645 – 26482021. https://doi.org/10.1016/j.matpr.2020.12.594.

[5] Y. Tsuboi, M. Goto, and A. Itaya, "Pulsed laser deposition of silk protein: Effect of photosensitized-ablation on the secondary structure in thin deposited films," *J. Appl. Phys.*, vol. 89, no. 12, pp. 7917–7923, 2001, doi: 10.1063/1.1371266.

[6] Fakhri M. A.; Abdulwahhab A. W.; Kadhim S. M.; Alwazni M. S.; Adnan S. A., Thermal oxidation effects on physical properties of CuO2 thin films for optoelectronic application, Materials Research Express, 6(2), 26429 (2019) 10.1088/2053-1591/aaf217.

[7] M. A. Hernandez-Perez, C. Garapon, C. Champeaux, P. Shahgaldian, A. Coleman, and J. Mugnier, "Pulsed laser deposition of bovine serum albumin protein thin films," *Appl. Surf. Sci.*, vol. 208–209, no. 1, pp. 658–662, 2003, doi: 10.1016/S0169-4332(02)01419-8.

[8] Muhammed, Q. Q., Saleh, M. M., Al-Azawi, R. J., Kadhim, A. C., Shaker, R. M., Close-Range Photogrammetric Techniques for Investigating and Documenting The Ancient Buildings, Optics InfoBase Conference Papers, 2022, JTu5A.91.

[9] K. Maximova, X. Wang, and A. Balˇ, "Writing of bio-compatible silk patterns : 3D laser nano-printing," pp. 8–9, 2016.

[10] Salih, M. M., Investigation of the effect of electromagnetic radiation on human health using remote sensing technique, International Journal of Safety and Security EngineeringThis link is disabled., 2021, 11(1), pp. 117–122.

[11] Salim E. T.; Awayiz M. T.; Mahdi R. O., Tea concentration effect on the optical, structural, and surface roughness of Ag2 O thin films, Digest Journal of Nanomaterials and Biostructures, 14(4), 1151-1159 (2019).

[12] F. G. Omenetto and D. L. Kaplan, "A new route for silk," Nat. Photonics, vol. 2, no. 11, pp. 641–643, 2008, doi: 10.1038/nphoton.2008.207.

[13] Fakhri M. A.; Salim E. T.; Tariq S. M.; Ibrahim R. K.; Alsultany F. H.; Alwahib A. A.; Alhasan S. F. H.; Gopinath S. C. B.; Salim Z. T.; Hashim U., A gold nanoparticles coated unclad single mode fiber-optic sensor based on localized surface plasmon resonance, Scientific Reports, 13(1), 5680 (2023) 10.1038/s41598-023-32852-6.

[14] Al Wazny M. S.; Salim E. T.; Bader B. A.; Fakhry M. A., Synthesis of Bi2O3 films, studying their optical, structural, and surface roughness properties, IOP Conference Series: Materials Science and Engineering, 454(1), 12160 (2018) 10.1088/1757-899X/454/1/012160.

[15] P. Cebe et al., "Beating the heat-fast scanning melts silk beta sheet crystals," Sci. Rep., vol. 3, pp. 1–7, 2013, doi: 10.1038/srep01130.

[16] Ismail R. A.; Salim E. T.; Halbos H. T., Preparation of Nb2O5 nanoflakes by hydrothermal route for photodetection applications: The role of deposition time, Optik, 245, 167778 (2021) 10.1016/j.ijleo.2021.167778.

[17] Alsultany F. H.; Alhasan S. F. H.; Salim E. T., Seed Layer-Assisted Chemical Bath Deposition of Cu2O Nanoparticles on ITO-Coated Glass Substrates with Tunable Morphology, Crystallinity, and Optical Properties, Journal of Inorganic and Organometallic Polymers and Materials, 31(9), 3749-3759 (2021) 10.1007/s10904-021-02016-y.

[18] P. Domachuk, H. Perry, J. J. Amsden, D. L. Kaplan, and F. G. Omenetto, "Bioactive 'self-sensing' optical systems," Appl. Phys. Lett., vol. 95, no. 25, 2009, doi: 10.1063/1.3275719.

[19] Awayiz M. T.; Salim E. T., Silver oxide nanoparticle, effect of chemical interaction temperatures on structural properties and surface roughness, AIP Conference Proceedings, 2213, 20247 (2020) 10.1063/5.0000215.

[20] H. J. Jin and D. L. Kaplan, "Mechanism of silk processing in insects and spiders," Nature, vol. 424, no. 6952, pp. 1057–1061, 2003, doi: 10.1038/nature01809.

[21] Awayiz M. T.; Salim E. T., Photo voltaic properties of Ag2O/Si heterojunction device: effect of substrate conductivity, Materials Science Forum, 1002, 200-210 (2020) 10.4028/www.scientific.net/MSF.1002.200.

[22] Abdul Muhsien M.; Salem E. T.; Agool I. R., Preparation and characterization of (Au/n-Sn O2 /Si O2 /Si/Al) MIS device for optoelectronic application, International Journal of Optics, 2013, 756402 (2013) 10.1155/2013/756402.

[23] L. D. Koh et al., "Structures, mechanical properties and applications of silk fibroin materials," Prog. Polym. Sci., vol. 46, pp. 86–110, 2015, doi: 10.1016/j.progpolymsci.2015.02.001.

[24 Khawla S. Khashan, Aseel A. Hadi, Rana O. Mahdi & Doaa S. Jubair, Aluminum-doped zinc oxide nanoparticles prepared via nanosecond Nd: YAG laser ablation in water: optoelectronic properties, Opt Quant Electron 56, 125 (2024). https://doi.org/10.1007/s11082-023-05630-x.

[25] S. Kapoor and S. C. Kundu, "Silk protein-based hydrogels: Promising advanced materials for biomedical applications," Acta Biomater., vol. 31, pp. 17–32, 2016, doi: 10.1016/j.actbio.2015.11.034.

[26] Jurn Y. N.; Malek F.; Mahmood S. A.; Liu W.-W.; Fakhri M. A.; Salih M. H., Modelling and simulation of rectangular bundle of single-walled carbon nanotubes for antenna applications Key Engineering Materials, 701, 57-66 (2016) 10.4028/www.scientific.net/KEM.701.57.

[27] Fakhri M. A.; Wahid M. H. A.; Kadhim S. M.; Badr B. A.; Salim E. T.; Hashim U.; Salim Z. T., The structure and optical properties of Lithium Niobate grown on quartz for photonics application, EPJ Web of Conferences, 162, 1005 (2017) 10.1051/epjconf/201716201005.

[28] B. Kundu, R. Rajkhowa, S. C. Kundu, and X. Wang, "Silk fibroin biomaterials for tissue regenerations," Adv. Drug Deliv. Rev., vol. 65, no. 4, pp. 457–470, 2013, doi: 10.1016/j.addr.2012.09.043.

[29] Roaa A. Abbas, Evan T. Salim & Rana O. Mahdi, Deposition time effect on copper oxide nano structures, an analysis study using chemical method, J Mater Sci: Mater Electron 35, 427 (2024). https://doi.org/10.1007/s10854-024-12143-0.

[30] J. Melke, S. Midha, S. Ghosh, K. Ito, and S. Hofmann, "Silk fibroin as biomaterial for bone tissue engineering," Acta Biomater., vol. 31, pp. 1–16, 2016, doi: 10.1016/j.actbio.2015.09.005.

[31] Khawla S khashan, Rana O Mahdi, Ban A. Badr, Farah Mahdi, Preparation and characterization of ZnMgO nanostructured materials as a photodetector, Journal of Physics: Conference Series 1795 (2021) 012008. doi:10.1088/1742-6596/1795/1/012008

[32] D. Aytemiz and T. Asakura, "Biotechnology of Silk," vol. 5, pp. 69–85, 2014, doi: 10.1007/978-94-007-7119-2.

[33] Aseel A. Hadi, Juhaina M. Taha, Rana O. Mahdi, Khawla S. Khashan, Influence of laser pulse on properties of NiO NPs prepared by laser ablation in liquid, AIP Conf. Proc. 2213, 020308 (2020) https://doi.org/10.1063/5.0000115.

[34] B. D. Lawrence et al., "Effect of hydration on silk film material properties," Macromol. Biosci., vol. 10, no. 4, pp. 393–403, 2010, doi: 10.1002/mabi.200900294.

[35] Evan T. Salim, Ahmed T. Hassan, Rana O Mahdi, Forat H. Alsultany, Physical Properties of HfO2 Nano Structures Deposited using PLD, IJNeaM, vol. 16, no. 3, pp. 495–510, Oct. 2023.

[36] T. Yucel, M. L. Lovett, and D. L. Kaplan, "Silk-based biomaterials for sustained drug delivery," J. Control. Release, vol. 190, pp. 381–397, 2014, doi: 10.1016/j.jconrel.2014.05.059.

[37] Azzam Y. kudhur, Evan T. Salim, Ilker Kara, Rana O. Mahdi & Raed K. Ibrahim, The effect of laser energy on Cu2O nanoparticles formation by liquid-phase pulsed laser ablation, J Opt 53, 1309–1321 (2024). https://doi.org/10.1007/s12596-023-01319-2.

[38] L. Zhou, G. Sun, K. Zhao, X. Wang, and A. Hu, "Generalized Cassie-Baxter equation for wetting of a spherical droplet within a smooth and heterogeneous conical cavity," vol. 4, no. 2, pp. 31–40, 2017.

[39] Hassen H. H.; Salim E. T.; Taha J. M.; Mahdi R. O.; Numan N. H.; Khalid F. G.; Fakhri M. A., Fourier transform infrared spectroscopy and photo luminance results for Zno NPs prepared at different preparation condition using LP-PLA technique, International Journal of Nanoelectronics and Materialsm, 11(Special Issue BOND21) 65-72 (2018).

[40] T. Fabritius, R. Myllylä, S. Makita, and Y. Yasuno, "Wettability characterization method based on optical coherence tomography imaging.," Opt. Express, vol. 18, no. 22, pp. 22859–22866, 2010, doi: 10.1364/OE.18.022859.

[41] Fakhri M. A.; Al-Douri Y.; Bouhemadou A.; Ameri M., Structural and Optical Properties of Nanophotonic LiNbO3 under Stirrer Time Effect, Journal of Optical Communications, 39(3), 297-306 (2018) 10.1515/joc-2016-0159.

[42] N. Eustathopoulos, M. G. Nicholas, and B. B. Drevet, Wettability at high temperatures, vol. 3. 1999.

[43] Jurn Y. N.; Malek F.; Mahmood S. A.; Liu W.-W.; Gbashi E. K.; Fakhri M. A., Important parameters analysis of the single-walled carbon nanotubes composite materials, ARPN Journal of Engineering and Applied Sciences, 11(8), 5108-5113 (2016).

[44] G. Bracco and B. Holst, Surface science techniques, vol. 51, no. 1. 2013.

[45] Rana O. Mahdi, Aseel A. Hadi, Juhaina M. Taha, Khawla S. Khashan, Preparation of nickel oxide nanoparticles prepared by laser ablation in water, AIP Conf. Proc. 2213, 020309 (2020) https://doi.org/10.1063/5.0000116.

[46] S. Ilican, M. Caglar, and Y. Caglar, "Determination of the thickness and optical constants of transparent indium-doped ZnO thin films by the envelope method," Mater. Sci., vol. 25, no. 3, pp. 709–718, 2007.

[47] Mohammed D. A.; Kadhim A.; Fakhri M. A., The enhancement of the corrosion protection of 304 stainless steel using Al2O3 films by PLD method, AIP Conference Proceedings, 2045, 20014 (2018) 10.1063/1.5080827.

[48] Fakhri M. A.; Numan N. H.; Mohammed Q. Q.; Abdulla M. S.; Hassan O. S.; Abduljabar S. A.; Ahmed A. A., Responsivity and response time of nano silver oxide on silicon heterojunction detector, International Journal of Nanoelectronics and Materials, 11(Special Issue BOND21), 109-114 (2018).

[49] K. Seo, M. Kim, and D. H. Kim, "Re-derivation of Young 's Equation , Wenzel Equation , and Cassie-Baxter Equation Based on Energy Minimization".

[50] Roaa A. Abbas, Evan T. Salim & Rana O. Mahdi, Morphology transformation of Cu2O thin film: different environmental temperatures employing chemical method, J Mater Sci: Mater Electron 35, 1057 (2024). https://doi.org/10.1007/s10854-024-12823-x.

[51] Fakhri M. A.; Numan N. H.; Alshakhli Z. S.; Dawood M. A.; Abdulwahhab A. W.; Khalid F. G.; Hashim U.; Salim E. T., Physical investigations of nano and micro lithium-niobate deposited by spray pyrolysis technique, AIP Conference Proceedings, 2045, 20015 (2018) 10.1063/1.5080828.

[52] K. J. Kubiak, M. C. T. Wilson, T. G. Mathia, and P. Carval, "Wettability versus roughness of engineering surfaces," Wear, vol. 271, no. 3–4, pp. 523–528, 2011, doi: 10.1016/j.wear.2010.03.029.

[53] Tawfiq Z. H.; Fakhri M. A.; Adnan S. A., Photonic Crystal Fibres PCF for Different Sensors in Review, IOP Conference Series: Materials Science and Engineering, 454(1), 12173 (2018) 10.1088/1757-899X/454/1/012173.

[54] D. Terada, Y. Yokoyama, S. Hattori, H. Kobayashi, and Y. Tamada, "The outermost surface properties of silk fibroin films reflect ethanol-treatment conditions used in biomaterial preparation," Mater. Sci. Eng. C, vol. 58, pp. 119–126, 2016, doi: 10.1016/j.msec.2015.07.041.

[55] Roaa A. Abbas, Evan T. Salim & Rana O. Mahdi, Morphology transformation of Cu2O thin film: different environmental temperatures employing chemical method, J Mater Sci: Mater Electron 35, 1057 (2024). https://doi.org/10.1007/s10854-024-12823-x.

[56] Fakhri M. A.; Wahid M. H. A.; Badr B. A.; Kadhim S. M.; Salim E. T.; Hashim U.; Salim Z. T., Enhancement of Lithium Niobate nanophotonic structures via spin-coating technique for optical waveguides application, EPJ Web of Conferences, 162, 1004 (2017) 10.1051/epjconf/201716201004.

[57] V. M. Swinerd, A. M. Collins, N. J. V. Skaer, T. Gheysens, and S. Mann, "Silk inverse opals from template-directed β-sheet transformation of regenerated silk fibroin," Soft Matter, vol. 3, no. 11, p. 1377, 2007, doi: 10.1039/b711975e.

[58] Azzam Y. Kudhur, Evan T. Salim, Ilker Kara, Makram A. Fakhri & Rana O. Mahdi, Structural optical and morphological properties of copper oxide nanoparticles ablated using pulsed laser ablation in liquid, J Opt 53, 1936–1945 (2024). https://doi.org/10.1007/s12596-023-01331-6.

[59] Doaa A. Mahmoud, Evan T. Salim, Rana O. Mahdi, A. Mindil, Subash C. B. Gopinath & Motahher A. Qaeed, Laser Ablation of Tungsten Metal for Au@WO3 Core-Shell Formation: A Characterizing Study at Different Laser Fluences, Plasmonics (2024). https://doi.org/10.1007/s11468-024-02607-8.

[60] I. Ghaeli et al., "Phase behaviour and miscibility studies of collagen/silk fibroin macromolecular system in dilute solutions and solid state," Molecules, vol. 22, no. 8, 2017, doi: 10.3390/molecules22081368.

[61] Muhsien M. A.; Salem E. T.; Agool I. R.; Hamdan H. H., Gas sensing of Au/n-SnO2/p-PSi/c-Si heterojunction devices prepared by rapid thermal oxidation, Applied Nanoscience (Switzerland), 4(6), 719-732 (2014) 10.1007/s13204-013-0244-7.

[62] A. F. Mohammed et al., "Ablation threshold measurements and surface modifications of 193 nm laser irradiated 4H-SiC," Chem. Phys. Lett., vol. 713, no. September, pp. 194–202, 2018, doi: 10.1016/j.cplett.2018.09.057.

[63] Fakhri M. A.; Bader B. A.; Khalid F. G.; Numan N. H.; Abdulwahhab A. W.; Hashim U.; Salim E. T.; Munshid M. A.; Salim Z. T., Optical and morphological studies of LiNbO3 nano and micro photonic structural, AIP Conference Proceedings, 2045, 20017 (2018) 10.1063/1.5080830.

[64] Jehan A. Saimon, Suzan N. Madhat, Khawla S. Khashan, Azhar I. Hassan, Rana O. Mahdi, Rafah A. Nasif, Synthesis of CdxZn1-xO nanostructure films using pulsed laser deposition technique, AIP Conf. Proc. 2045, 020003 (2018) https://doi.org/10.1063/1.5080816.

[65] Q. A. Al-Jarwany et al., "Realisation of a sub-wavelength dimple using a 193 nm wavelength photonic nano jet," Chem. Phys. Lett., vol. 750, no. January, p. 137400, 2020, doi: 10.1016/j.cplett.2020.137400.

[66] Fakhri M. A.; Abdulwahhab A. W.; Dawood M. A.; Raheema A. Q.; Numan N. H.; Khalid F. G.; Wahid M. H. A.; Hashim U.; Salim E. T., Optical investigations of nano lithium niobate deposited by spray pyrolysis technique with injection of Li2CO3 and Nb2O5 as raw materials, International Journal of Nanoelectronics and Materials, 11(Special Issue BOND21), 103-108 (2018).

[67] Alsultany F. H.; Alhasan S. F. H.; Salim E. T., Seed Layer-Assisted Chemical Bath Deposition of Cu2O Nanoparticles on ITO-Coated Glass Substrates with Tunable Morphology, Crystallinity, and Optical Properties, Journal of Inorganic and Organometallic Polymers and Materials, 31(9), 3749-3759 (2021) 10.1007/s10904-021-02016-y.

[68] A. Sagnella et al., "Effect of different fabrication methods on the chemo-physical properties of silk fibroin films and on their interaction with neural cells," RSC Adv., vol. 6, no. 11, pp. 9304–9314, 2016, doi: 10.1039/c5ra20684g.

[69] Fakhri M. A.; Salim E. T.; Wahid M. H. A.; Salim Z. T.; Hashim U., A novel parameter effects on optical properties of the LiNbO3 films using sol-gel method, AIP Conference Proceedings, 2213, 20242 (2020) 10.1063/5.0000206.

[70] Q. A. Al-Jarwany, A. A. Aesa, A. F. Mohammed, and C. D. Walton, "Wettability measurements of agarose thin films patterned by 193 nm ArF excimer laser," Indian J. Phys., 2024, doi: 10.1007/s12648-024-03345-7.